

tively. The minimum velocity  $\beta_{\min}$  in the two-sided case can be shown to be

$$\beta_{\min} = \begin{cases} \beta_{\text{app}}/2 & \text{if } \beta_{\text{app}} \leq \sqrt{2} \\ (\beta_{\text{app}}^2 - 1)^{1/2}/\beta_{\text{app}} & \text{if } \beta_{\text{app}} > \sqrt{2} \end{cases}$$

giving a corresponding range of values of 0.5 to 0.8. This expression assumes only equal and opposite velocities for the two components. Simultaneous ejection is not required and the core can lie anywhere between the two separating components. In either geometry, the intrinsic motion in the radio source is therefore at least mildly relativistic.

Extrapolating the outermost subcomponents backwards in time at the observed separation speed, we derive the zero separation time of August  $13.5 \pm 0.5$ . This is roughly one day after the rapid rise in the radio flux density<sup>3</sup> and close to the end of the decline of the X-ray luminosity<sup>11</sup>. This is a most peculiar aspect of the behaviour of GRO J1655–40 and makes it unique among Galactic X-ray sources. The appearance of the radio outburst 12 days after the X-ray outburst, when the X-ray flux decreased strongly, suggests that the mechanism which formed the X-rays also inhibited the formation and ejection of the radio components. The accretion of material onto a compact object offers a plausible explanation if initially the accretion disk is geometrically thick and radiation-pressure supported, emitting X-rays at essentially the Eddington limit during a supercritical accretion event, then becomes thin and stable after the accretion rate decreases. Thus, while the accretion rate was high and the disk thick, the formation and ejection of radio components was disrupted, with at best only a weak, optically thick radio component present. Once the disk became thin and stabilized, the ejection events could occur by well known mechanisms such as Blandford–Payne<sup>12</sup>. This is consistent with the observed X-ray flux during the outburst, which remained constant at roughly the level corresponding to the Eddington limit for an object of 1 solar mass at a distance of  $\sim 4$  kpc.

The identification of moving radio components in GRO J1655–40, along with those in GRS1915+105, SS433 and Cyg X–3 (ref. 13), indicates that such behaviour may not be uncommon in Galactic X-ray objects. Furthermore, it seems that a continuum of intrinsic speeds, currently known to range from  $0.25c$  in SS433 to  $0.92c$  in GRS1915+105, may characterize this new class of source. The link between relativistic motion and the possible signature of accretion, the delay of the emergence of the radio components until the decline of the X-ray luminosity in GRO J1655–40, may be an important clue to the nature of radio component production, not only in these objects, but also in the much more luminous and massive objects in active galactic nuclei. The detection of superluminal motion and the familiar jet or knot morphology in Galactic sources is itself important, and suggests an underlying unity of mechanism over an enormous range in scale, from the galaxy-scale outbursts seen in quasars and active galactic nuclei, to their comparatively feeble and smaller analogue seen here in GRO J1655–40.  $\square$

12. Blandford, R. D. & Payne, D. G. *Mon. Not. R. astr. Soc.* **199**, 883–903 (1982).  
13. Spencer, R. E., Swinney, R. W., Johnston, K. J. & Hjellming, R. M. *Astrophys. J.* **309**, 694–699 (1986).

ACKNOWLEDGEMENTS. We thank the Observatory Directors for allowing these observations to be scheduled at short notice, and the NASA Deep Space Network for making time available at Tidbinbilla and Goldstone. The Australia Telescope is operated as a national facility by CSIRO. Part of this research was carried out at the Jet Propulsion Laboratory, under contract to NASA. S.J.T. and J.E.J.L. are supported by an Australian Postgraduate Research Award.

## Antibody catalysis of a reaction otherwise strongly disfavoured in water

Doron Shabat\*, Harel Itzhaky\*,  
Jean-Louis Reymond† & Ehud Keinan\*†‡

\* Department of Chemistry, Technion-Israel Institute of Technology, Technion City, Haifa 32000, Israel

† Department of Molecular Biology, The Scripps Research Institute, 10666 North Torrey Pines Road, La Jolla, California 92037, USA

SEVERAL examples have been reported recently<sup>1</sup> of antibody catalysis<sup>2</sup> of reactions that are strongly disfavoured because of the high free energy of the transition state. Here we show that catalytic antibodies can be used to promote a particularly useful kind of reaction from a synthetic point of view: one involving an intermediate that is highly unstable in water. We show that an antibody elicited against the quaternary ammonium ion 4a (Fig. 1) catalyses the protonation of the enol ether 1 to form, with complete enantioselectivity, an oxocarbenium intermediate. This species is highly reactive in water, and would normally react with a water molecule to give the corresponding ketone 2. But the antibody provides a hydrophobic environment that allows the oxocarbenium ion instead to undergo an intramolecular reaction to form an enantiomerically pure ketal 3. This result shows that catalytic antibodies can exclude solvent molecules entirely from crucial steps on the reaction pathway.

Oxocarbenium ion intermediates such as I (Fig. 1) and the glycosyl cation have lifetimes in water in the order of  $10^{-5}$ – $10^{-12}$  s (refs 3, 4). In the acid-catalysed hydrolysis of enol ether 1, the rate-determining step with the transition state of highest energy is the formation of intermediate I (Fig. 1). Partitioning of I to yield products 2 and 3 occurs after the rate-determining step and involves lower energy barriers<sup>5,6</sup>. Thus, for a catalyst to promote ketal formation, it should be able both to lower the energy barrier between enol ether 1 and intermediate I, and to lower the energy barrier for conversion of I to ketal 3 relative to ketone 2.

Monoclonal antibody 14D9, which binds hapten 4a with high affinity, catalyses several reactions involving oxocarbenium ion intermediates, including cleavage of a cyclic acetal<sup>7</sup>, hydrolysis of ketals<sup>8</sup>, and hydrolysis of enol ethers<sup>9</sup>. The latter reaction proceeds with high enantioselectivity of protonation at carbon and can be done on a preparative scale<sup>10</sup>. Catalysis occurs through stabilization of the intermediate oxocarbenium ion by an ionizable protein side chain<sup>9</sup>. A notable part of the binding energy between 14D9 and hapten 4a is provided by hydrophobic interactions with the methylpiperidinium moiety of the hapten, which implies that the antibody active site is highly hydrophobic<sup>11</sup>. We therefore expected that this antibody might not only catalyse the formation of intermediate I by protonation of enol ether 1, but could also influence the partitioning step and lead to formation of ketal 3 by excluding water from the reaction centre.

Received 14 October 1994; accepted 31 January 1995.

- Mirabel, I. F. & Rodriguez, L. F. *Nature* **371**, 46–48 (1994).
- Zhang, S. N. et al. *IAU Circ.* No. 6046 (1994).
- Campbell-Wilson, D. & Hunstead, R. *IAU Circ.* No. 6052 (1994).
- Jauncey, D. L. et al. in *Very High Angular Resolution Imaging* (eds Robertson, J. & Tango, W.) 131–133 (Kluwer, Dordrecht, 1994).
- Preston, R. A. et al. in *Sub-Arcsecond Radio Astronomy* (eds Davis, R. J. & Booth, R. J.) 428–430 (Cambridge Univ. Press, 1993).
- Vermeulen, R. C., Schilizzi, R. T., Icke, V., Fejes, I. & Spencer, R. E. *Nature* **328**, 309–313 (1987).
- Della Valle, M. *IAU Circ.* No. 6052 (1994).
- Crawford, I. A., Barlow, M. J. & Blades, J. C. *Astrophys. J.* **336**, 212–230 (1989).
- Caswell, J. L., Murray, J. D., Roger, R. S., Cole, D. J. & Cooke, D. J. *Astr. Astrophys.* **45**, 239–258 (1975).
- Pearson, T. J. & Zensus, J. A. in *Superluminal Radio Sources* (eds Pearson, T. J. & Zensus, J. A.) 1–11 (Cambridge Univ. Press, 1987).
- Wilson, C. A. et al. *IAU Circ.* 6056 (1994).

‡ To whom correspondence should be addressed.

Acid-catalysed hydrolysis of enol ether 1 in aqueous solution gives ketone 2 as the sole product. No traces of ketal 3 can be detected, indicating that the substrate's hydroxyl group cannot compete against water on intermediate I. Antibody 14D9 catalyses the hydrolysis of 1. Catalysis is totally inhibited by hapten 4b and follows saturation kinetics. Although the catalytic reactions are done in 100% aqueous medium, about 12% of ketal 3 is found in the reaction products. Formation of products 2 and 3 follows Michaelis–Menten kinetics (Fig. 2), yielding comparable  $K_m$  values. This suggests that both the ketone and ketal products originate from a common intermediate that is formed catalytically in the antibody combining site.

The ratio between ketone 2 and ketal 3 formed in the antibody-catalysed reaction is constant throughout a broad pH

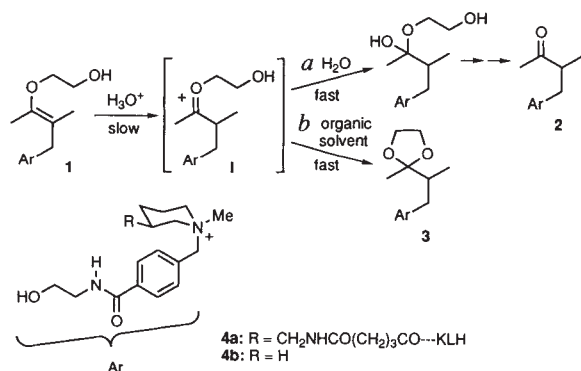


FIG. 1 Oxocarbenium ion intermediate I is generated by protonation of enol ether 1 under acid catalysis. In aqueous media, I is rapidly trapped by a molecule of water to yield a hemiketal and ultimately ketone 2 (pathway a). In organic solvents, under very low concentration of water, I can undergo ring closure to produce ketal 3 (pathway b). Although proton transfer is the rate-determining step in the overall conversion of 1 to either 2 or 3, the relative proportions of the two products is highly dependent on the medium. Monoclonal antibody 14D9, which binds hapten 4a with high affinity, catalyses the hydrolysis of 1 in 100% aqueous medium to produce a mixture of 2 and 3. Catalysis is totally inhibited by 4b and follows saturation kinetics.

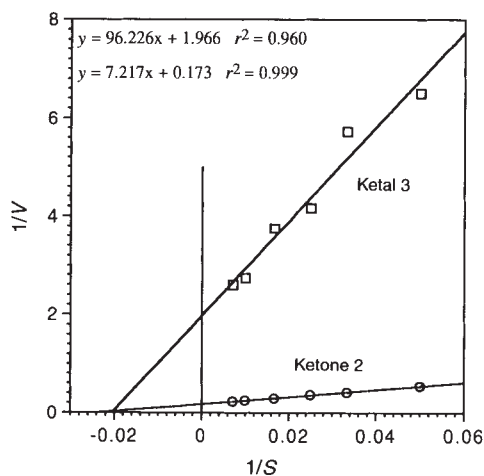


FIG. 2 A Lineweaver–Burk plot for the 14D9-catalysed hydrolysis of 1 to 2 and 3. General assay conditions: antibody (2–5  $\mu\text{M}$ ), substrate (20–150  $\mu\text{M}$ ), either PBS or 1,3-bis(tris(hydroxymethyl)-methylamino)propane buffered saline (50 mM buffer, 100 mM NaCl) at 25 °C. All reactions were monitored at 254 nm by reverse-phase high-performance liquid chromatography (RP-HPLC; Hitachi L-6200A equipped with an AS-2000 autosampler and a Supelcosil LC-18 column (25 cm  $\times$  4.6 mm, 5 m) using 20:80 acetonitrile:water at 1 ml min<sup>-1</sup>. All data shown here (rate,  $V$ , s<sup>-1</sup>; concentration,  $S$ ,  $\mu\text{M}$ ) were obtained from reactions in PBS, pH 6.06, with the calculated  $K_m$  values for formation of compounds 2 and 3 being 42 and 50  $\mu\text{M}$ , respectively. For the combined products:  $K_{\text{cat}} = 1.2 \times 10^{-3}$ ,  $K_{\text{uncat}} = 2.0 \times 10^{-6}$  s<sup>-1</sup>.

range (between 5 and 9). Similarly, this product distribution is independent of the reaction temperature between 4 and 37 °C. These observations suggest that the mechanistic pathways leading from intermediate I to either ketone or ketal are almost identical in terms of acid–base mechanism as well as thermodynamic activation parameters.

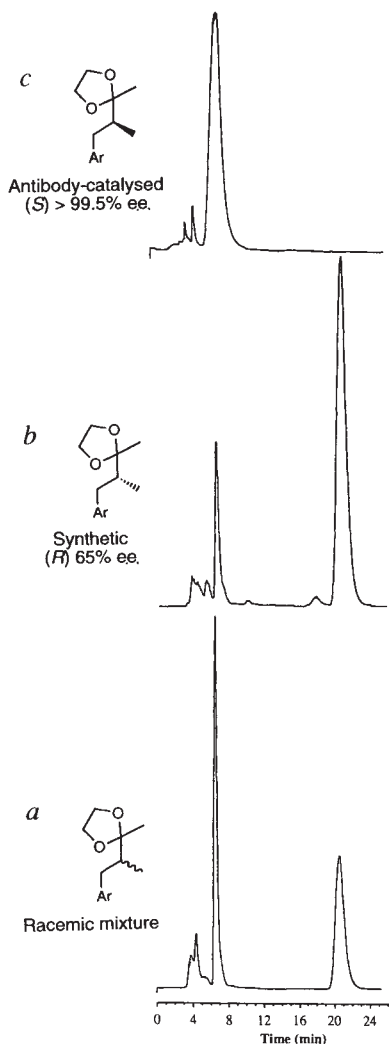


FIG. 3 Determination of absolute configuration and enantiomeric purity of ketal 3 produced in the antibody 14D9-catalysed reaction of 1. All analyses were done by HPLC (Perkin-Elmer 410 equipped with an ultraviolet detector, 254 nm) using a Chiracell OD-H column (Daicel Chemical Industries) with 20:80 isopropanol:hexane at a flow rate of 1 ml min<sup>-1</sup>. a, HPLC chromatogram of a racemic mixture of 3. b, Chromatogram of (R)-3 that was synthesized from enantiomerically pure (1R, 2S)-(-)-norephedrine using the Evans methodology, proceeds with high diastereoselectivity and predictable absolute configuration<sup>15</sup>. The absolute configuration at the homobenzylic position was assigned on the basis of the many examples reported by Evans, including a closely related asymmetric alkylation reaction with unsubstituted benzyl bromide. c, Chromatogram of 3 that was produced by 14D9-catalysed reaction (note that a peak corresponding to the (R)-enantiomer cannot be detected even when the column is overloaded with a concentrated sample that causes peak broadening). As shown here, ketal 3 is obtained from the antibody-catalysed reaction with (S) configuration in >99.5% e.e. Similar HPLC analysis of ketone 2 isolated from the same antibody-catalysed reaction shows that it is formed with (S) configuration in 80% e.e. Considering that 20% of 2 is formed by the competing hydronium ion-catalysed hydrolysis of 1 under the reaction conditions, as determined by a control experiment, the observed enantiomeric purity of 2 (80% e.e.) implies that the reaction taking place in the antibody active site proceeds with greater than 97% enantioselectivity.

Both products 2 and 3 isolated from the same antibody-catalysed reaction are obtained with high enantiomeric purity and with the same (*S*) absolute configuration (Fig. 3). The remarkably high enantiomeric purity of ketal 3 (>99.5% enantiomeric excess, e.e.) agrees with the fact that 3 is formed exclusively by antibody catalysis. Furthermore, it also represents the first direct proof that the rate-determining protonation at carbon is achieved with complete enantioselectivity in the antibody active site. These observations confirm the assumption that both ketal 3 and ketone 2 originate from partitioning of a single intermediate and not from two diastereoisomeric transition states, which could be formed by protonation at either of the prochiral faces of the double bond in enol ether 1.

To assess the difficulty of what antibody catalysis has accomplished we have studied model systems. Formation of ketal 3 reflects low availability of water molecules at the vicinity of the intermediate I in the antibody active site. Such a medium effect is expected to exist within the hydrophobic active site of antibody 14D9<sup>9,11</sup>. To test this hypothesis we used mixtures of either dioxane-water or isopropanol-water containing 5% acetic acid as a simple model environment<sup>12</sup>. Acetic acid was chosen to mimic the residue responsible for general acid catalysis in the antibody active site. Measurable proportions of ketal are formed only at very low water concentration in acidic dioxane (Fig. 4a). The situation is even worse in acidic isopropanol, where less than 1% ketal could be detected at water concentrations greater than 1%. The product distribution of the antibody reaction corresponds to that observed in acidic dioxane containing only 3% water.

Very similar dependence of ketal proportions on water concentration is observed when perchloric acid ( $5 \times 10^{-4}$  M) is used as the catalyst instead of acetic acid in either dioxane or isopropanol (both solutions, 5% acetic acid in water and  $5 \times 10^{-4}$  M perchloric acid in water, have pH 3.5), clearly showing that the partitioning is independent of the acid catalyst used. Similarly, reaction rates with HClO<sub>4</sub> decline by four orders of magnitude with decreased water concentration (from 100 to 5%). However, rates are increased steeply by one order of magnitude at lower concentration of water in both solvents (data not shown). This rate increase reflects enhanced reactivity of the hydronium ion as it becomes solvated by cosolvents which are less basic than water. This superacidity effect is not observed with acetic acid because acetate is more basic than water and therefore buffers the reactivity of the proton. Although the ionizable side chain responsible for catalysis in the antibody active site ( $pK_a = 5.8$ )<sup>9,13</sup> should buffer the reactivity of the hydronium ion, a similar superacidity effect might explain part of the unusual rate enhancement observed with this catalyst.

Reaction rates drop by four orders of magnitude in these media as compared with pure water (Fig. 4b). By contrast, the antibody accelerates the reaction by three orders of magnitude. Attribution of ketal formation in the antibody active site to an effect of the medium would therefore lead to the conclusion that the antibody actually accelerates the reaction by seven orders of magnitude. Although the approximation of the antibody active site to a homogeneous, isotropic medium may be an oversimplification, this model is consistent with the observation of constant ketal/ketone ratios over broad ranges of pH values and temperatures.

As to the origin of ketal formation in the water-dioxane system, it is probably a dual effect of both lowered concentration of water molecules and increased alcohol nucleophilicity due to desolvation. Although the same factors could operate in the antibody active site as well, one should also consider the highly organized, asymmetrical environment within that site which may restrict the available conformations of intermediate I and thereby control its partitioning.

One of the greatest advantages of natural enzymes is their ability to handle reactive intermediates under ambient temperatures in the presence of water. For example, formation of a

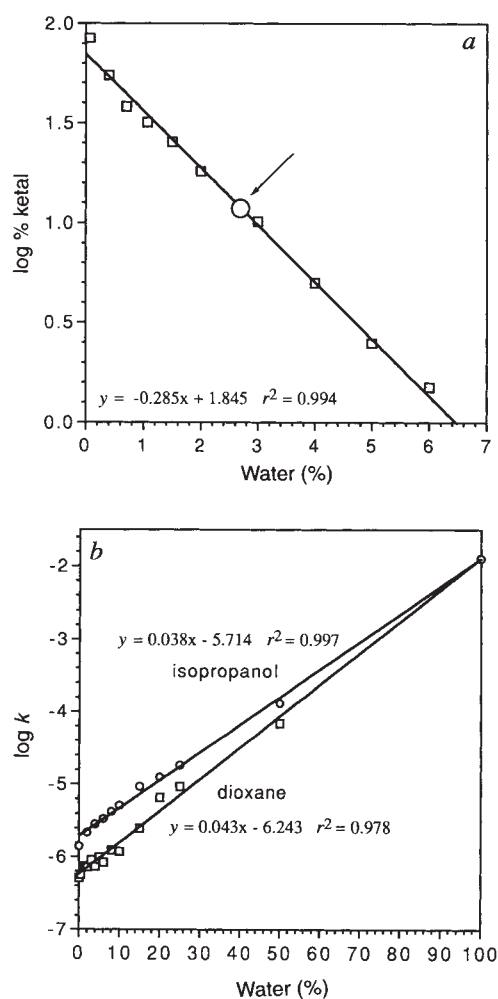


FIG. 4 Uncatalysed hydrolysis of 1 in organic solvents. *a*, Effect of water concentration on yields of ketal 3. All reactions were at 24 °C with  $10^{-4}$  M substrate 1, using varying mixtures of dioxane and water and a constant concentration (5% v/v) of acetic acid. The circular data point represents the 12% ketal formed in the antibody-catalysed reaction. On this line it corresponds to 2.7% water in dioxane/acetic acid. *b*, Effect of water concentration on the reaction rate; log rate constants ( $s^{-1}$ ) of the reaction either in isopropanol (circular data points) or in dioxane (rectangular points).

glycosidic bond by organic synthesis requires strictly anhydrous conditions in order to prevent hydrolysis of the highly reactive glycosyl cation. Glycosyl transferases, however, catalyse the same reactions in water<sup>14</sup>. We have shown here that it is possible to generate and handle water-incompatible, highly reactive intermediates within the active site of a catalytic antibody in aqueous solution. This has been demonstrated by the very difficult chemical task of ketal formation in water. The isolation of ketal 3 in very high enantiomeric purity is a striking example of the potential use of such chemistry. This proves that the 14D9-catalysed protonation at carbon is absolutely enantioselective. A wide array of synthetic transformations involving other water-incompatible, reactive intermediates should now be considered for antibody catalysis. □

Received 30 November 1994; accepted 10 February 1995.

- Lerner, R. A., Benkovic, S. J. & Schultz, P. G. *Science* **252**, 659–667 (1991).
- Schultz, P. G. & Lerner, R. A. *Acc. Chem. Res.* **26**, 391–395 (1993).
- Banait, N. S. & Jencks, W. P. *J. Am. chem. Soc.* **113**, 7951–7958 (1991).
- Pothier, N., Goldstein, S. & Deslongchamps, P. *Helv. chim. Acta* **75**, 604–620 (1992).
- Jenks, W. P. *Catalysis in Chemistry and Enzymology* 52–60 (Dover, New York, 1987).
- Schmir, G. L. & Gunningham, B. A. *J. Am. chem. Soc.* **87**, 5692–5700 (1965).
- Reymond, J.-L., Janda, K. D. & Lerner, R. A. *Angew. Chem. int. Ed. engl.* **30**, 1711–1713 (1991).

8. Sinha, S. C., Keinan, E. & Reymond, J.-L. *Proc. natn. Acad. Sci. U.S.A.* **90**, 11910–11913 (1993).
9. Reymond, J.-L., Jahangiri, G. K., Stoudt, C. & Lerner, R. A. *J. Am. chem. Soc.* **115**, 3909–3917 (1993).
10. Reymond, J.-L., Reber, J.-L. & Lerner, R. A. *Angew. Chem. int. Ed. engl.* **33**, 475–477 (1994).
11. Jahangiri, G. K. & Reymond, J.-L. *J. Am. chem. Soc.* **116**, 11264–11274 (1994).
12. Lewis, C., Paneth, P., O'leary, M. H. & Hilvert, D. *J. Am. chem. Soc.* **115**, 1410–1413 (1993).
13. Sinha, S. C., Keinan, E. & Reymond, J.-L. *J. Am. chem. Soc.* **115**, 4893–4894 (1993).
14. Schuster, M., Wang, P., Paulson, J. C. & Wong, C.-H. *J. Am. chem. Soc.* **116**, 1135–1136 (1994).
15. Evans, D. A., Ennis, M. D. & Mathre, D. J. *J. Am. chem. Soc.* **104**, 1737–1739 (1982).

ACKNOWLEDGEMENT. We thank the US-Israel Binalational Science Foundation and the US National Institutes of Health for financial support.

## Increase in lower-stratospheric water vapour at a mid-latitude Northern Hemisphere site from 1981 to 1994

S. J. Oltmans & D. J. Hofmann

NOAA Climate Monitoring and Diagnostics Laboratory, 325 Broadway, Boulder, Colorado 80303, USA

WATER vapour in the atmosphere is the key trace gas controlling weather and climate, and plays a central role in atmospheric chemistry, influencing the heterogeneous chemical reactions that destroy stratospheric ozone. Although in the upper troposphere and lower stratosphere the radiative<sup>1</sup> and chemical<sup>2</sup> effects of water vapour are large, there are few measurements of water-vapour concentration<sup>3–10</sup> and its long-term variation<sup>11–13</sup> in this region. Here we present a set of water-vapour profiles for altitudes from 9 to 27 km, obtained at Boulder, Colorado, during 1981–94, which show a significant increase in water-vapour concentration in the lower stratosphere over this time. The increase is larger, at least below about 20–25 km, than might be expected from the stratospheric oxidation of increasing concentrations of atmospheric methane<sup>14,15</sup>. The additional increase in water vapour may be linked to other climate variations, such as the observed global temperature rise in recent decades<sup>16</sup>.

In global climate models, nearly half of the projected increase in temperature due to a doubling of carbon dioxide in the atmosphere results from the effects of increased water vapour<sup>17</sup>. A doubling of water vapour in the stratosphere could lead to a 1 °C increase in surface temperature<sup>18</sup>. The present radiative forcing from the estimated rise in stratospheric water vapour resulting from methane oxidation is calculated<sup>16</sup> to be about 10% of that for CO<sub>2</sub>. But our limited knowledge of water vapour in the upper troposphere and lower stratosphere is one of the main uncertainties in climate modelling<sup>19</sup>.

Chemically, water vapour is the primary source of the hydroxyl radical in the atmosphere<sup>20</sup>. Recent work<sup>21,22</sup> has shown that water vapour concentration determines the effectiveness of the heterogeneous reactions that destroy ozone in the lower stratosphere. An increase in water vapour could thus lead to greater ozone loss.

The measurement of water vapour in the drier portions of the atmosphere, particularly above 5–10 km, is difficult<sup>3–6</sup>. The inability of standard radiosondes to obtain such measurements and the generally high cost of suitable techniques has left a data gap in this region. Recently, satellite<sup>7,9</sup> and aircraft measurements<sup>10</sup> have shed new light on the variation of water vapour over a broader expanse of the globe, particularly in the stratosphere but also in the upper troposphere. Longer-term records of water vapour in this region are rare and limited to a few locations<sup>11–13</sup>.

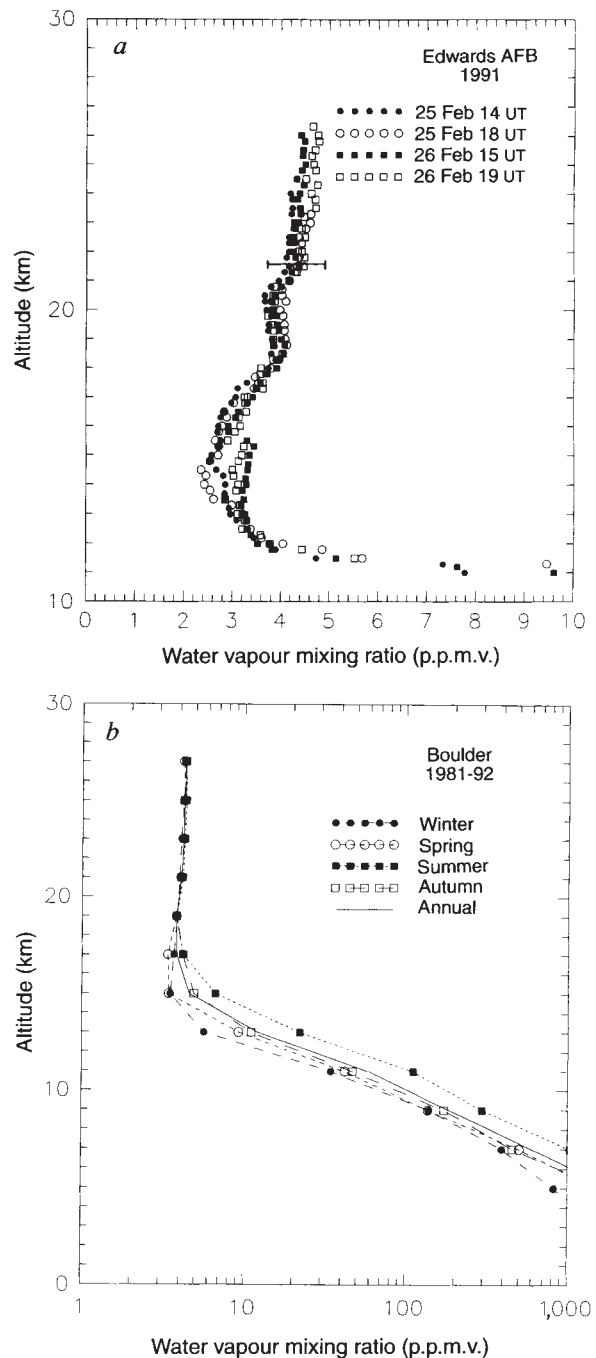


FIG. 1 Vertical profile mixing ratios for water vapour, in parts per million by volume (p.p.m.v.). *a*, At Edwards Air Force Base (AFB), California, for four soundings done within about a 30-h period in February 1991; *b*, for the seasonal and annual averages in the stratosphere at Boulder, Colorado, for the period 1981–94. In *a*, horizontal bar plotted at 21.5 km is  $\pm 15\%$  of the mean and represents a conservative estimate of the instrument error. Above 18 km the symbol size in *b* represents one standard deviation about the mean.

The water-vapour profiles in this work were obtained using balloon-borne frost-point hygrometers. The instrument is a chilled-mirror design which uses a liquid cryogen, giving fairly fast response for an instrument of this type<sup>11,23</sup>. The cryogen provides ample cooling to make measurements to altitudes of at least 30 km. The hygrometer operates on the principle that an equilibrium exists between the vapour pressure in the atmosphere and a water or ice surface only at a unique temperature (the dew or frost-point temperature). Using the Goff–Gratch<sup>24</sup> relationship, the mixing ratio of water vapour (relative to the